ChemPubSoc
Europe

▍ **Spin Crossover**

Stabilization of the Low-Spin State in a Mononuclear Iron(II) Complex and High-Temperature Cooperative Spin Crossover Mediated by Hydrogen Bonding

Sipeng Zheng,[a] Niels R. M. Reintjens,[a] Maxime A. Siegler,[b] Olivier Roubeau,[c] Elisabeth Bouwman,[a] Andrii Rudavskyi,[d] Remco W. A. Havenith,[d, e] and Sylvestre Bonnet*[a]

Abstract: The tetrapyridyl ligand bbpya (bbpya $=$ N,N-bis(2,2′-bipyrid-6-yl)amine) and its mononuclear coordination compound [Fe(bbpya)(NCS)$_2$] (**1**) were prepared. According to magnetic susceptibility, differential scanning calorimetry fitted to Sorai's domain model, and powder X-ray diffraction measurements, **1** is low-spin at room temperature, and it exhibits spin crossover (SCO) at an exceptionally high transition temperature of $T_{1/2} = 418$ K. Although the SCO of compound **1** spans a temperature range of more than 150 K, it is characterized by a wide (21 K) and dissymmetric hysteresis cycle, which suggests cooperativity. The crystal structure of the LS phase of compound **1** shows strong N$-$H···S intermolecular H-bonding interactions that explain, at least in part,

the cooperative SCO behavior observed for complex **1**. DFT and CASPT2 calculations under vacuum demonstrate that the bbpya ligand generates a stronger ligand field around the iron(II) core than its analogue bapbpy ($N,N′$-di(pyrid-2-yl)-2,2′-bipyridine-6,6′-diamine); this stabilizes the LS state and destabilizes the HS state in **1** compared with [Fe(bapbpy)(NCS)$_2$] (**2**). Periodic DFT calculations suggest that crystal-packing effects are significant for compound **2**, in which they destabilize the HS state by about 1500 cm^{-1}. The much lower transition temperature found for the SCO of **2** compared to **1** appears to be due to the combined effects of the different ligand field strengths and crystal packing.

Introduction

Spin crossover (SCO) concerns the switching of 3d^4–3d^7 transition-metal ions between a high-spin state (HS) and a low-spin state (LS).[1] It can be triggered by temperature variations, light irradiation, or the application of pressure, a magnetic field, or an electric field.[2] In cooperative SCO materials, the change in spin state of a particular metal ion is influenced by the spin state of its neighbors,[3] which may lead, at the macroscopic level, to abrupt transitions and hysteresis. Cooperativity is a very important aspect of SCO as it is required in many technological applications that would involve SCO, such as displays or memory devices.[4] However, it is difficult to design cooperative SCO materials with transitions that occur at or above room temperature.[5] Coordination polymers, such as iron(II)/1,2,4-triazole[6] and Hofmann networks of the type [Fe^{II}(μ-$N,N′$-bis-diimine)M(μ-CN)$_4$][7] (M$=$Cu, Ni, Pt, Au, Ag) are classical examples of cooperative SCO compounds in which the bridging ligands allow for efficient communication between the iron centers. However, in such coordination polymers, the ions situated at the boundaries of a crystalline domain may experience a different environment than the ions in the bulk, which can be detrimental to SCO nanomaterials.[8] In contrast, mononuclear compounds offer a well-defined coordination environment throughout the whole solid. Nevertheless, molecular compounds with cooperative transitions occurring near or above room temperature remain scarce.[5, 9–15] On the one hand the ligand set must stabilize the LS state of iron(II); on the other hand it should allow very strong supramolecular interactions to counter-balance the natural narrowing of hysteresis cycles when the transition temperature of the SCO increases.[16]

[a] Dr. S. Zheng, N. R. M. Reintjens, Prof. E. Bouwman, Dr. S. Bonnet
Leiden Institute of Chemistry, Gorlaeus Laboratories
Leiden University, P.O. Box 9502, Leiden, 2300 RA (The Netherlands)
E-mail: bonnet@chem.leidenuniv.nl

[b] Dr. M. A. Siegler
Small Molecule X-ray Facility, Department of Chemistry
Johns Hopkins University, Baltimore, MD 21218 (USA)

[c] Dr. O. Roubeau
Instituto de Ciencia de Materiales de Aragón (ICMA)
CSIC and Universidad de Zaragoza
Plaza San Francisco s/n, 50009 Zaragoza (Spain)

[d] A. Rudavskyi, Prof. R. W. A. Havenith
Theoretical Chemistry, Zernike Institute for Advanced Materials
University of Groningen, Nijenborgh 4, 9747 AG Groningen
(The Netherlands)

[e] Prof. R. W. A. Havenith
Stratingh Institute for Chemistry, University of Groningen,
Nijenborgh 4, 9747 AG Groningen, The Netherlands
and
Ghent Quantum Chemistry Group, Department of Inorganic and Physical
Chemistry, Ghent University, Krijgslaan 281 (S3), 9000 Gent (Belgium)

⌨ Supporting information for this article (powder X-ray diffractograms and IR spectra at room temperature for **1**, intermolecular distances in the crystal structure of **1** (LS phase), derivative of χ_MT versus T plot for complex **1**, and bond distances and angles of the minimized structures) is available on the WWW under http://dx.doi.org/10.1002/chem.201503119.

A seminal SCO paper[4] even stated that "if [SCO] molecules are hydrogen-bonded, [intermolecular] interactions may be enhanced, but remain insufficient to give rise to a strong cooperativity." Herein, we describe a new molecular SCO compound, [Fe(bbpya)(NCS)2] (1) (bbpya = N,N-bis(2,2′-bipyrid-6-yl)amine), that simultaneously shows an exceptionally high transition temperature, high cooperativity, and intermolecular H-bonding, and we demonstrate with theoretical calculations that the bbpya ligand stabilizes the LS state of the iron(II) complex.

Inspired by earlier investigations on the two-step SCO compound [Fe(bapbpy)(NCS)2] (2) (bapbpy = N,N′-di(pyrid-2-yl)-2,2′-bipyridine-6,6′-diamine),[17] the new rigid N_4-donor ligand bbpya was designed (Figure 1). This tetradentate ligand con-
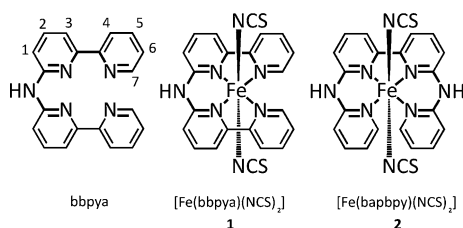
Figure 1. The bbpya ligand, its iron complex **1**, and the analogue compound [Fe(bapbpy)(NCS)2] (**2**).[17] Proton numbering scheme is shown for NMR attributions.

sists of two bipyridine units connected by an N—H bridge. In metal thiocyanato complexes of this ligand, this N—H bridge aims at forming intermolecular N—H⋯S hydrogen bonds, which have been shown to be critical for the cooperativity of bapbpy-based SCO compounds.[18] The bbpya ligand is structurally similar to the bapbpy ligand and is expected to coordinate to the iron(II) ion in a tetradentate fashion, which would leave two *trans* axial positions for the binding of thiocyanate ions. However, bbpya also differs from bapbpy: it has only one N—H bridge and, upon coordination, forms two five-membered rings and one six-membered ring, whereas bapbpy has two N—H bridges and forms one five-membered ring and two six-membered rings (Figure 1). The presence of two bpy (bipyridine) chelates and the overall more open structure of bbpya are expected to result in a reduced distortion of the coordination sphere of iron(II) and an increase in the ligand field splitting, which would lead to a stabilization of the LS state.

Results and Discussion

The bbpya ligand was obtained in 69% yield by a Buchwald–Hartwig cross-coupling reaction between 6-amino-2,2′-bipyridine[19,20] and 6-bromo-2,2′-bipyridine (Scheme 1). The reaction of bbpya with 1.1 equiv of Fe(NCS)2 in MeOH resulted in a deep purple suspension, which was stirred overnight and filtered to afford compound **1** as a deep purple powder. The dark color of the compound suggested a low-spin state at room temperature. Single crystals suitable for X-ray structure determination were grown using liquid–liquid diffusion of a methanolic solution of [Fe(NCS)2] into a DMF solution of
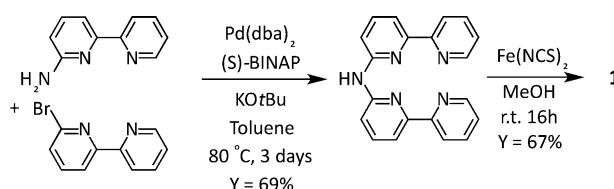
Scheme 1. Synthetic route towards the ligand bbpya and its iron complex **1**.

bbpya. The powder X-ray diffraction pattern calculated from the single-crystal data determined at 110(2) K matched the experimental powder X-ray diffractogram of compound **1** at 298 K. Furthermore, identical IR spectra were obtained for the crude powder and for the single crystals (Supporting Information, Figures S1 and S2). Overall, at room temperature and below, both the crystals and the powder sample of **1** were made up of the same phase of the same compound.

Compound **1** crystallizes in the triclinic space group $P\bar{1}$. At 110(2) K, the structure of complex **1** is wholly disordered, and the major and minor components of the disorder are related through a pseudo inversion center (occupancy factor of the major component: 0.7038(15)). The coordination geometry and bond lengths in the two orientations are highly similar, but the two orientations have a major impact on the long-range hydrogen-bonding interactions (see below). As anticipated, the Fe(II) ion exists in an octahedral geometry with four N-donors of the ligand bbpya sitting in the equatorial plane and two N-donors of the thiocyanate anions in the axial positions. The crystal lattice does not contain any solvent molecules. A projection of complex **1** is shown in Figure 2 (see Table 1 for selected bond lengths and angles). At 110 K, the average Fe—N
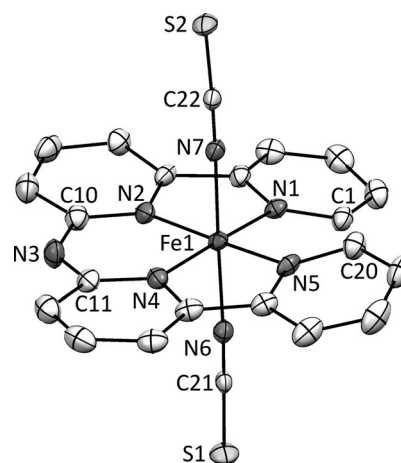
Figure 2. Displacement ellipsoid plot, set at 50% probability level, of compound **1** at 110(2) K. Hydrogen atoms and the minor component of the disorder are omitted for clarity.

bond length is 1.96 Å, which is typical for a LS Fe(II) complex in an octahedral environment and is comparable to those found for complex **2** in the LS phase (Fe—N_{avg} = 1.95 Å).[17] The angle between the two planes of the two terminal pyridine rings is 22.8° in **1**, which is significantly smaller than that
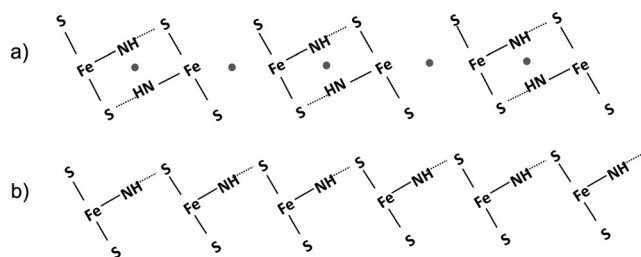
Table 1. Selected bond lengths [Å] and angles [°] for the crystal structure of **1** at 110(2) K.[a]

Fe1—N1	1.996(4)	N3···S2	3.321(4)	N6—Fe1—N7	178.48(12)
Fe1'—N1'	1.975(10)			N6'—Fe1'—N7'	179.5(4)
Fe1—N2	1.934(4)	N3'···S1'	3.084(7)	N1—N2—N4—N5	9.3(2)
Fe1'—N2'	1.952(9)			N1'—N2'—N4'—N5'	10.8(5)
Fe1—N4	1.948(4)	N3'···S2'	3.286(14)	C1—N1—N5—C20	25.8(3)
Fe1'—N4'	1.963(10)			C1'—N1'—N5'—C20'	22.1(8)
Fe1—N5	1.995(3)	N1—Fe1—N2	81.91(17)	N2—C10—C11—N4	2.1(3)
Fe1'—N5'	1.954(9)	N1'—Fe1'—N2'	82.1(4)	N2'—C10'—C11'—N4'	0.9(8)
Fe1—N6	1.943(4)	N2—Fe1—N4	94.70(16)	C20—C11—C10—C1	11.77(7)
Fe1'—N6'	1.958(10)	N2'—Fe1'—N4'	93.3(4)	C20'—C11'—C10'—C1'	11.3(2)
Fe1—N7	1.932(4)	N4—Fe1—N5	81.62(17)		
Fe1'—N7'	1.945(10)	N4'—Fe1'—N5'	82.0(5)		
N3···S1	3.107(10)	N5—Fe1—N1	102.38(16)		
		N5'—Fe1'—N1'	103.4(5)		

[a] Short intermolecular interactions [Å] of complex **1** are also provided.

found in **2** (44.8°).[17] The more planar orientation of the coordinated bbpya ligand is most likely due to the replacement of one of the six-membered metallacycles in **2** by a five-membered metallacycle in **1** (see above). Unlike in complex **2**, in **1** the angles between the vectors Fe1—N6 or Fe1—N7 and the mean molecular plane, which is defined by N1, N2, N4, and N5, are 82.5 or 84.2°, respectively; that is, the axial thiocyanate ligands are approximately perpendicular to the mean molecular plane of the bbpya ligand. Side views of the molecular geometries of complexes **1** and **2** at 110 K (Supporting Information, Figure S4) show that the structure of complex **1** has indeed a much less distorted octahedron shape than complex **2**.
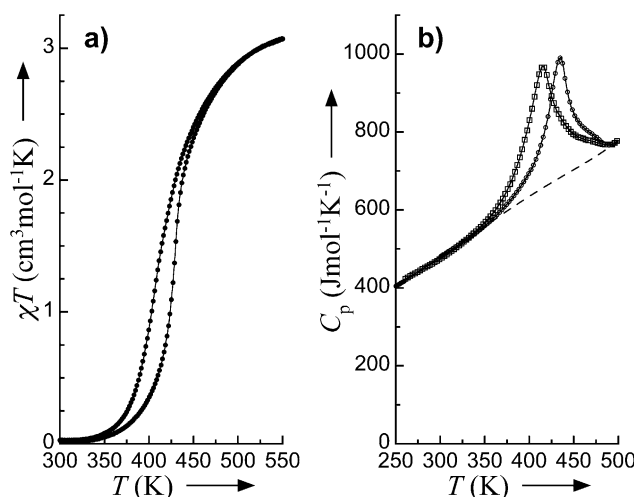
In the crystal structure of **1**, the Fe complexes are disordered (Supporting Information, Figure S3). Disorder may occur during nucleation and crystal growth because of competitive N—H···S hydrogen-bond interactions as each molecule has two potential H-bond acceptors (S1 and S2) but only one potential H-bond donor (N3). Optimization of hydrogen-bond interactions in the crystal structure can be achieved through two distinct H-bond networks: 1) centrosymmetric H-bond dimers (mode **a**) and 2) 1D H-bond chains (mode **b**; Figure 3). In mode **a**, the network is built of hydrogen-bonded dimers with two strong N—H···S hydrogen bonds (N3···S2 and N3'···S2'). The lack of one

extra N—H donor in the bbpya ligand prevents the propagation of hydrogen bonds along one direction. In mode **b**, the network is achieved through 1D chains that feature two unidirectional hydrogen bonds (N3···S1' and N3'···S1). In both modes, only one thiocyanate group is an acceptor in one N—H···S interaction. The H-bonded network in the crystal structure of complex **1** is a combination of both modes **a** and **b** so that, statistically, both thiocyanate groups can be acceptors in N—H···S hydrogen bonds. As the Fe complexes are disordered, the propagation of N—H···S hydrogen bonds can be achieved through a set of unidirectional N—H···S hydrogen bonds that occur successively between the major and minor components of the disorder along the [101] plane, which form "···major···minor···major···" 1D chains. However, these hydrogen-bonded chains have defects because of the statistical distribution of the molecules over their disordered components. Finally, weak π—π stacking interactions might also occur between the complexes **1**, as shown by the short distances between the centroids Cg1 and Cg2' of the terminal pyridine rings of two neighboring molecules (Cg1···Cg2' = 4.28 Å; Supporting Information, Figure S5). Overall, in the crystal structure of complex **1**, the propagation of strong intermolecular interactions can still be achieved in the long-range order despite the presence of a single N—H bridge per molecule. Therefore, the intermolecular interactions that we observed in the crystal structure of complex **1**, based on the assumption that complex **1** has SCO properties, suggest that it may show cooperativity.

To investigate the magnetic properties of **1**, the temperature dependence of $\chi_M T$ was measured in the range 300–550 K on a powder sample of compound **1** (χ_M is the molar magnetic susceptibility and T the temperature; Figure 4a). $\chi_M T$ data show that **1** undergoes a complete SCO that, like non-cooperative compounds, spans over 150 K. However, it also shows a wide (21 K) hysteretic cycle, which is characteristic of strongly cooperative compounds. At room temperature and up to about 330 K, the $\chi_M T$ value of 0.01–0.02 cm^3 mol^{-1} K is clearly indicative of a LS state, which is consistent with the dark color of the compound and the short Fe—N distances that were experimentally determined by single-crystal X-ray crystallography. Further heating of the sample to 550 K in an oven was neces-

Figure 3. Representations of the two limiting contact modes between adjacent molecules in the crystal packing of **1**. In mode **a**, the H-bond network is best described as centrosymmetric H-bond dimers, but there is no propagation of H-bonding interactions in the crystal. In mode **b**, the propagation of H-bonding interactions is achieved in the crystal. In both modes, only one of the two thiocyanate groups is H-bond acceptor. The H-bond network in compound **1** is a combination of modes **a** and **b** (see text). Inversion centers are indicated by dots.

Figure 4. a) Thermal variation of $\chi_M T$ for **1**. b) Molar heat capacities for **1** upon warming (○) and cooling (□). The dashed line is the estimated normal heat capacity used for ΔC_p determination. All measurements were performed at 10 K min^{-1}.

Figure 5. Powder X-ray diffractograms (PXRD) for compound **1** at a) 553 K and b) 297 K. Both PXRD in the heating and cooling modes are identical at 297 K. All PXRD were taken in vacuum (6×10^{-2} mbar) to prevent aerial oxidation.

sary to reach the $\chi_M T$ value of 3.02 cm^3 mol^{-1} K that is expected for an Fe(II) ion in its HS state. A strongly dissymmetric hysteresis cycle of 21 K at its widest point was reproduced over several heating/cooling cycles, which shows that it is not the result of irreversible phase transitions or decomposition. The SCO occurs at $T_{1/2}\uparrow = 428(1)$ upon warming and $T_{1/2}\downarrow = 407(3)$ K upon cooling, which were derived from the maximum of d($\chi_M T$)/dT (Supporting Information, Figure S6). The average transition temperature $T_{1/2}$ is 418 K, and this is one of the highest transition temperatures reported for molecular SCO compounds.[9,10,21–25] Notably, it is remarkably higher than that of **2**, which, in spite of its similar molecular structure, is HS at room temperature and exhibits a two-step transition upon cooling.[17]

Attempts at the structural characterization of the HS state of complex **1** were undertaken. Challenges arise as the SCO temperature occurs at a temperature that is not commonly attainable with the temperature controller of most single-crystal X-ray diffractometers. However, the HS state could be characterized by high-temperature powder X-ray diffraction (PXRD) under vacuum (Figure 5). The diffractogram at 553 K revealed a higher symmetry compared to that at 297 K; the peaks at $2\theta = 18.7$, 23.3, and 24.8° disappeared, and the triplet at $2\theta = 20.3$, 21.0, and 21.9° turned into a more intense doublet at $2\theta = 19.6$ and 20.5°. These changes were reproduced without significant changes over several heating/cooling cycles between 297 K and 550 K, which showed that complex **1** undergoes a reversible thermal-phase transition that must correspond to SCO.

To support these data, differential scanning calorimetry (DSC) measurements were undertaken on a powder sample of compound **1** in the range 150–500 K. The calorimetric data revealed anomalies in both the warming and cooling modes at the temperatures $T_{1/2}\uparrow = 434(1)$ and $T_{1/2}\downarrow = 415(1)$ K, respectively, as defined by heat capacity maxima (Figure 4b). These temperatures clearly define a hysteresis cycle and match those of
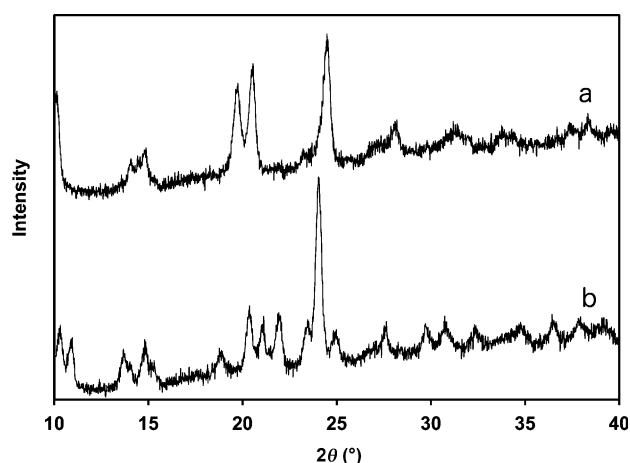
the transitions in the $\chi_M T$ versus T plot; therefore, they can be ascribed to a cooperative SCO phenomenon in **1**. The excess enthalpy and entropy that is associated with the SCO in complex **1** can be derived from integration of ΔC_p over T (Figure 6a) and ln T, respectively, which leads to $\Delta_{SCO}H = 12.9$,
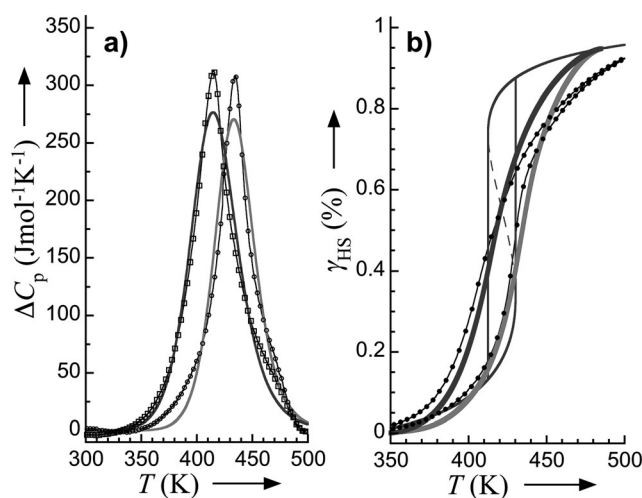
Figure 6. a) Excess molar heat capacities associated with the SCO in compound **1**. Bold light gray and dark gray lines are best-fits of the data upon warming (○) and cooling (□) to the domain model of Sorai[5–16] (see the Supporting Information) with $n = 10.2$ and 6.5, respectively. b) The SCO of compound **1** shown as the high-spin fraction γ_{HS} versus T (bold light gray and dark gray lines are derived from calorimetric data, black dots are from magnetic data), and the simulation with the Slichter–Drickamer model (thin gray line).

15.6 kJ mol^{-1} and $\Delta_{SCO}S = 29.9$, 37.4 J mol^{-1} K^{-1} upon warming and cooling, respectively. These relatively large values are in agreement with a cooperative SCO in **1**.[26,27] To quantify cooperativity, the excess heat capacity was fitted to Sorai's domain model (full lines in Figure 6a and see the Supporting Information).[28] The fit yielded $n = 10.2$ and 6.5 upon warming and

cooling, respectively, which represents the number of like-spin SCO centers per interacting domain. The former value is consistent with that obtained for the lower temperature transition observed in **2**, and with the cooperative transition of other reported SCO complexes [Fe(L)(NCS)$_2$], in which L is a disubstituted bapbpy derivative.[18] The latter, smaller value is consistent with the more gradual transition/broader excess heat capacity peak observed in other Fe(II) bapbpy-based complexes upon cooling.[18] For a direct comparison, HS fractions were derived from both magnetic and calorimetric data, which show an excellent agreement (Figure 6 b). Another quantification of the cooperative character of the SCO in compound **1** can be obtained from these data with the so-called Slichter–Drickamer model.[16] The best agreement was obtained with a mean-field interaction term $\Gamma = 8.15 \text{ kJ mol}^{-1}$. This result, which corresponds to $\Gamma/RT_{1/2} = 2.34$, is perfectly consistent with the experimental observations as, in this model, bistability is predicted for values of $\Gamma/RT_{1/2} > 2$, and the width of the resulting hysteresis cycle in the SCO curve increases with $\Gamma/RT_{1/2}$. Overall, powder X-ray diffraction, magnetic, and calorimetric data provided a consistent view of the spin transition of complex **1**. The observed hysteresis cycle, which is a sign of efficient cooperativity in compound **1**, is in agreement with the intermolecular interactions (H-bonding and π–π stacking) observed in the crystal packing.

Quantum chemical calculations were utilized to determine if the difference in transition temperature between **1** and **2** was due to either the different stabilization of the LS state by the bbpya and bapbpy ligands or the crystal-packing effects that may induce effective pressure, which would shift ΔE and the transition temperature.[29, 30] First, DFT geometry optimizations for both complexes were performed in vacuum (see the Supporting Information, Table S1 for Fe—N distances). For the LS state of **2**, the Fe—N distances showed reasonable agreement with the crystal structure data (LS phase). For complex **1** a slight deviation was found: the theoretical structure possessed C_2 symmetry, whereas the experimental structure showed some differences from this. For the HS state of complex **2**, the geometrical features of the theoretical model deviated considerably from the experimentally observed structure, which may be caused by crystal-packing effects. For **1**, the experimentally determined HS crystal structure was not available, hence no comparison could be made, whereas periodic DFT geometry optimizations for complex **2** were performed by using the same functional and basis set and keeping the experimental unit cell parameters fixed (see the Supporting Information). Indeed, the structure that was optimized in the crystal lattice for complex **2** showed very good agreement with the experimental data (see the Supporting Information, Table S1). As the structural geometry that was obtained by optimization in vacuum deviated considerably from the experimental one, these results confirm the presence of crystal-packing effects in complex **2**, which may destabilize the HS state.

The HS–LS energy differences ΔE^0_{HL} were also calculated by using the DFT-minimized structures (Table 2). The zero-point vibrational corrections ΔZPE to the total energy were found in the range of −700 to −1000 cm^{-1}, which is typical for SCO ma-

Table 2. High-spin–low-spin energy differences [cm^{-1}] for **1** and **2** according to DFT and CASPT2 calculations.[a]

	[Fe(bapbpy)(NCS)$_2$] (**2**)		
Method	ΔE_{HL}	ΔZPE	ΔE^0_{HL}
DFT (PBE)	7590	−768	6822
CASPT2	−2819	–	−3587[b]
Periodic DFT	9064	–	–
Single-point DFT[c]	8792		

	[Fe(bbpya)(NCS)$_2$] (**1**)		
Method	ΔE_{HL}	ΔZPE	ΔE^0_{HL}
PBE (PBE)	9871	−937	8934
CASPT2	−830	–	−1767[b]

[a] ΔE^0_{HL} = electronic HS–LS energy difference; ΔZPE = zero-point vibrational correction to the HS–LS energy difference; $\Delta E^0_{HL} = \Delta E_{HL} + \Delta$ZPE. [b] Value obtained by using CASPT2 energy difference and DFT (PBE) zero-point vibrational correction. [c] On geometries optimized in the crystal.

terials.[31, 32] However, the absolute values of the DFT (PBE) energy differences ΔE_{HL} were found in the range of 7000–10000 cm^{-1}, which is much too high for SCO compounds with thermal SCO and would result in transition temperatures around 1000 K and higher (for example, [Fe(terpy)$_2$]$^{2+}$).[31] Periodically optimized structures for complex **2** showed that the HS–LS energy difference was about 1500 cm^{-1} larger than that recorded in vacuum. This result again confirmed the presence of crystal-packing effects for complex **2**, but did not fit to the experimental values of the transition temperatures found for both complexes **1** and **2**. Single-point DFT calculations performed on geometries of the complexes optimized in the crystal showed a similar HS–LS energy difference, which indicates that the crystal packing influences the HS–LS energy difference mainly through modification of the geometry. Upon going from the vacuum-optimized geometries to the geometries optimized in the crystal structure, the total energy of the LS-state complex was destabilized less than that of the HS-state geometry, which resulted in a larger ΔE^0_{HL} for the crystal structures. The most pronounced changes in the HS-state geometry by crystal packing were elongations of the Fe—NCS bonds and shortenings of the Fe—N1 bonds (see the Supporting Information, Table S1 and the geometries of the corresponding structures). This modification of the geometry also resulted in moderate changes of the orbital energies, although, owing to severe mixing of the iron d-orbitals with the ligand orbitals, it is difficult to conclusively say how these changes in orbital energies of the t$_{2g}$- and e$_g$-like iron d-orbitals affect the total energy difference.

The geometry and vibrational frequencies of SCO complexes are usually well reproduced by DFT, whereas the accurate determination of the HS–LS energy difference is a well-known problem of DFT as this is a single reference method that is incapable of a proper description of the multi-configurational nature of the spin states unless the functional is empirically reparametrized.[33, 34] To obtain accurate HS–LS energy differences ΔE^0_{HL}, ab initio methods have to be used, such as CASSCF/CASPT2, which is much more computationally demanding and

typically does not allow for the full geometry optimization for SCO materials, particularly in a crystal lattice. For this reason CASPT2 energy calculations were performed on the DFT geometries optimized in vacuum; the energies are presented in Table 2. The ΔE_{HL} and ΔE^0_{HL} values found for **1** and **2** were negative, which was in disagreement with the experimental observations as it would indicate that both complexes should remain in the HS state. However, these values confirmed the DFT results because, for complex **1**, the HS–LS energy difference was about 2000 cm^{-1} larger than for complex **2**. Overall, the fact that the energy difference ΔE^0_{HL} between the LS and HS state that was calculated by both methods in vacuum for compound **1** was about 2000 cm^{-1} larger than for compound **2** confirms that the stronger ligand field that was generated by bbpya around iron(II) stabilizes the LS state and destabilizes the HS state, relative to bapbpy. Thus, the bbpya ligand must play a significant contribution in the increase of the transition temperature for compound **1**, compared to **2**. Periodic DFT calculations show that crystal-packing effects were significant for compound **2**, in which they result in the destabilization of the HS state by about 1500 cm^{-1}. We may speculate that similar effects are present for compound **1**, but the absence of the crystal structure of the HS phase has prevented us, up to now, from performing similar calculations.

Conclusion

Ligand design aimed at replacing one six-membered ring in compound **2** with a 5-membered ring to increase the transition temperature of the SCO led to the new bis-bipyridine ligand bbpya and its iron complex **1**. Compound **1** not only showed SCO properties, but its transition temperature was remarkably enhanced (by ca. 200 K) compared with **2**. Hence, the LS state remained the most stable state of complex **1** at room temperature, whereas complex **2** was in a HS state at room temperature. Thus, the bbpya ligand offers a unique opportunity to stabilize the LS state of iron(II) complexes, which was further confirmed by DFT and CASPT2 calculations. In addition, although the number of N–H bridges per molecule of bbpya was reduced by a factor of 2 compared to bapbpy, disorder in **1** facilitated the propagation of H-bonding intermolecular interactions in the crystal lattice, which led to the formation of disordered, infinite supramolecular chains in the solid. Overall, compound **1** not only shows one of the highest transition temperatures recorded among mononuclear SCO complexes, but it also keeps a large (dissymmetric) hysteresis cycle of 21 K. These results suggest that hydrogen bonds can facilitate the propagation of intermolecular interactions, which lead to hysteresis in high-temperature molecular SCO materials. Furthermore, they open a unique opportunity to study the mechanism of cooperative SCO in molecular compounds as many experimental techniques (for example, near-field or optical microscopy) are easier to implement upon heating the sample above room temperature than upon cooling at cryogenic temperatures.

Experimental Section

All chemicals were obtained from commercial sources and used without further purification, unless otherwise mentioned. 6-Bromo-2,2′-bipyridine was purchased from Sigma-Aldrich (CAS 10495-73-5), and 6-amino-2,2′-bipyridine was synthesized according to previously reported procedures.[19, 20] Experiments that needed an inert environment were performed by using standard Schlenk techniques. The applied vacuum was about 10^{-3} mbar. Degassed solvents were obtained by bubbling argon through the solvent in a Schlenk flask for at least one hour. For all ligand and complex syntheses, degassed solvents were used; for ligand purifications, solvents were used without further purification. Complexes were filtered through Whatman RC 60 membrane filters. For other filtrations Whatman 597 filters were used. NMR spectra were measured on a Bruker DPX-300 spectrometer at room temperature. Mass spectra were obtained by using soft electron spray from a Thermoquest Finnagen AQA. High-resolution mass spectra were measured by using direct injection (2 μL of a 2 μM solution in DMSO) on a Thermo Finnigan LTQ Orbitrap mass spectrometer equipped with an electron spray ion source in positive mode (source voltage 3.5 kB, sheath gas flow 10, capillary temperature 275 °C) with resolution R = 60.000 at *m/z* 400 (mass range 150–2000) and dioctylphthalate (*m/z* 391.28428) as "lock mass". IR spectra were acquired on a PerkinElmer FT-IR Spectrum Two spectrometer at room temperature. Elemental analyses (C,H,N,S) were obtained on a Perkin-Elmer 2400 Series II analyzer.

Synthesis of bbpya

A mixture of 6-bromo-2,2′-bipyridine (250 mg, 1.07 mmol), [Pd(dba)$_2$] (13 mg, 0.022 mmol), (S)-BINAP (27 mg, 0.043 mmol), and KO*t*Bu (483 mg, 4.30 mmol) in a dry round-bottom flask under argon was partially dissolved in degassed toluene (20 mL). The mixture was stirred for 10 min, 6-amino-2,2′-bipyridine (220 mg, 1.28 mmol) was added, and the reaction mixture was heated to 80 °C. After 3 days, the brown mixture was cooled with an ice bath. Deionized water (25 mL) was added, and the mixture was stirred for 1 h. No solid appeared, and the resultant mixture was then extracted with CH$_2$Cl$_2$ (3×40 mL). The organic layers were combined, dried over MgSO$_4$, and filtered, and the solvent was evaporated under reduced pressure to give a brown oil. Cold MeOH was added to the oil, and the resultant solids were isolated by filtration, washed with cold MeOH, and dried under high vacuum to afford bbpya as a white solid (241 mg, 69%). R_f = 0.09 (SiO$_2$, 10% MeOH/CH$_2$Cl$_2$); ^{1}H NMR ([D$_6$]DMSO): δ = 9.90 (s, 1H, NH), 8.69 (ddd, *J* = 4.8, 1.9, 0.9 Hz, 2H, H-7), 8.38 (dt, *J* = 8.0, 1.1 Hz, 2H, H-4), 7.99 (td, *J* = 7.7, 1.8 Hz, 2H, H-6), 7.93 (dt, *J* = 5.4, 2.7 Hz, 2H, H-3), 7.89 (d, *J* = 2.9 Hz, 4H, H-1, H-2), 7.45 ppm (ddd, *J* = 7.5, 4.7, 1.2 Hz, 2H, H-5); ^{13}C NMR ([D$_6$]DMSO): δ = 155.5 (Cq), 153.9 (Cq), 153.4 (Cq), 149.3 (C-7), 138.9 (C-1), 137.3 (C-6), 124.0 (C-5), 120.4 (C-4), 112.8 (C-3), 112.3 ppm (C-2); ^{1}H NMR (CD$_2$Cl$_2$): δ = 8.72–8.61 (m, 2H), 8.40 (d, *J* = 8.0 Hz, 2H), 8.07–7.97 (m, 2H), 7.90–7.77 (m, 4H), 7.71 (d, *J* = 8.2 Hz, 2H), 7.54 (s, 1H), 7.32 (ddd, *J* = 7.4, 4.7, 1.1 Hz, 2H); IR (ATR): $\tilde{v}$ = 3390, 2922, 2852, 1582, 1558, 1520, 1472, 1447, 1418, 1340, 1296, 1271, 1230, 1152, 1091, 1073, 1050, 990, 963, 902, 818, 774, 738, 679, 668, 644, 620, 572, 402, 341, 317 cm^{-1}; MS (ESI, MeOH): *m/z* calcd for [*M*+H]$^+$ (326.4); found: 0326.1, [*M*+Na]$^+$ (348.4); found: 348.0, [2*M*+Na]$^+$ (673.2); found: 673.7; elemental analysis calcd (%) for C$_{20}$H$_{15}$N$_5$: C 73.82, H 4.65, N 21.53; found: C 73.21, H 5.36, N 20.39.

Preparation of [Fe(bbpya)(NCS)$_2$](1)

An Fe(NCS)$_2$ solution was prepared by weighing KSCN (195 mg, 2.00 mmol) and ascorbic acid (6.1 mg, 0.035 mmol) under argon into a round-bottom flask. FeSO$_4$ (152 mg, 1.00 mmol) was added and the mixture was suspended in degassed methanol (6.0 mL). The suspension was stirred for 40 min and then filtered. The filtrate was transferred into a volumetric flask, and the volume was adjusted to 10.0 mL with degassed methanol and the volumetric flask was well shaken, which yielded a 0.1 M [Fe(NCS)$_2$] solution in methanol. As the filtrate and the iron solution were not kept under argon, the iron solution had to be freshly prepared for every synthesis. The oxidation of the iron solution was visible by a change of color (from colorless to dark violet).

The ligand bbpya (30 mg, 0.093 mmol) was dissolved in degassed methanol (3.0 mL) in a round-bottom flask and stirred under argon to give a yellow solution. The [Fe(NCS)$_2$] solution (1.1 equiv, 0.1 mmol, 0.1 M) was added to the dissolved ligand, and the mixture was stirred 16 h under argon. The resultant purple solid was collected by filtration, washed with degassed methanol (3×5 mL), and dried under high vacuum for 3 h (31 mg, 67%). ^{1}H NMR ([D$_6$]DMSO): $\delta = 9.92$ (s, 1H), 8.68 (d, $J = 3.9$ Hz, 2H), 8.38 (d, $J = 7.7$ Hz, 2H), 8.06–7.80 (m, 6H), 7.46 (dd, $J = 6.8$, 4.7 Hz, 2H), 6.34 ppm (s, 1H), integration of the peaks was difficult due to the low solubility of the complex; IR (ATR): $\tilde{v} = 3269$, 3184, 3130, 3099, 3047, 2125 (NCS$^-$), 2109 (NCS$^-$), 1625, 1601, 1582, 1529, 1478, 1464, 1451, 1416, 1406, 1302, 1250, 1172, 1164, 1139, 1090, 1022, 949, 870, 800, 759, 725, 685, 661, 643, 629, 495, 478 cm^{-1}; HRMS (ESI, DMSO): m/z calcd for [M]$^+$: 497.0174; found: 497.0170, [M−NCS]$^+$: 439.0423; found: 439.0420; elemental analysis calcd (%) for C$_{22}$H$_{15}$FeN$_7$S$_2$: C 53.13, H 3.04, N 19.73, S 12.87; found: C 52.56, H 2.93, N 19.73, S 12.77.

Growing single crystals of compound 1

The ligand bbpya (15 mg) was dissolved in degassed DMF (3 mL) to afford a clear yellow solution. A small amount of ascorbic acid (5 mg) was added to prevent aerial oxidation. 1 mL aliquots of this solution were pipette-filtered over 1 cm Celite into the vertical compartment of a Y-shaped glass tube, Fe(NCS)$_2$ (0.5 mL of a 0.1 M solution) was carefully added into the other compartment of the glass tube. Liquid nitrogen was used to freeze both compartments before degassed MeOH was added to fill the Y-shaped tubes. Each tube was stoppered and kept at room temperature under argon by using balloons and leaving in a sunny place if possible as light seemed to aid crystallization. Single crystals were obtained within a week. Yield: 90%. The crystals were not air-sensitive and did not break because of loss of solvent; therefore, they could be handled out of the mother liquor and at ambient conditions for several weeks.

Crystal data: Fw = 497.38, black irregular lath, 0.43 × ×0.12 × 0.08 mm^3; triclinic; space group $P\bar{1}$ (no. 2); $a = 8.8024(4)$, $b = 8.8862(4)$, $c = 13.7229(5)$ Å; $\alpha = 100.637(3)$, $\beta = 103.916(3)$, $\gamma = 95.972(3)°$; $V = 1011.52(8)$ Å^3; $Z = 2$; $D_x = 1.633$ g cm^{-3}; $\mu = 8.134$ mm^{-1}; $T_{min} - T_{max}$ range: 0.195–0.596. 12241 reflections were measured up to a resolution of $(\sin \theta / \lambda)_{max} = 0.62$ Å^{-1}; 3945 reflections were unique ($R_{int} = 0.0215$), of which 3502 were observed [$I > 2\sigma(I)$]; 404 parameters were refined by using 102 restraints; R1/wR2 [$I > 2\sigma(I)$]: 0.0315/0.0818; R1/wR2 [all refl.]: 0.0357/0.0850; S = 1.074; residual electron density found between −0.30 and 0.23 e Å^{-3}.

Details of single-crystal X-ray structure determination

All reflection intensities were measured at 110(2) K by using a SuperNova diffractometer (equipped with Atlas detector) with Cu$_{K\alpha}$ radiation ($\lambda = 1.54178$ Å) under the program CrysAlisPro (Version 1.171.36.28 Agilent Technologies, 2013). The program CrysAlisPro was used to refine the cell dimensions and for data reduction. The structure was solved with the program SHELXS-2013[35] and was refined on F^2 with SHELXL-2013.[35] Analytical numeric absorption corrections based on a multifaceted crystal model were applied using CrysAlisPro. The temperature of the data collection was controlled by using the system Cryojet (manufactured by Oxford Instruments). The H atoms were placed at calculated positions by using the instructions AFIX 43 with isotropic displacement parameters, which have values 1.2×U_{eq} of the attached C or N atoms. The Fe complex was disordered over two orientations (Supporting Information, Figure S3), and both components of the disorder were related by a pseudo-inversion center. The occupancy factor of the major component of the disorder was refined to 0.7038(15). To keep the data-to-parameter ratio to an acceptable level, the EADP constraints were used for all disordered atoms that were related by inversion symmetry (no EADP constraints were applied to the heaviest atoms Fe and S). CCDC 1019880 contains the supplementary crystallographic data for this paper. These data are provided free of charge by The Cambridge Crystallographic Data Centre.

Additional note: The structure was initially solved in the space group $P1$ (no. 1) with $Z' = 2$. However, the ADDSYM procedure in PLATON[47] suggested a missed inversion center and the space group $P\bar{1}$ (no. 2). Another warning sign for choosing the wrong space group $P1$ was the value of the Flack parameter,[48] which refined exactly to 0.5. A refinement measured by using a racemic twin model with the transformation matrix (−1 0 0/0 −1 0/0 0 −1) did not improve the model much, and the structure remained significantly disordered in $P1$. An additional check for twinning was done by using the TwinRotMat procedure in PLATON, but no twin law could be detected. Eventually, the structure was solved and refined in the space group $P\bar{1}$ (no. 2).

Magnetic susceptibility measurements

Magnetic measurements were performed on a powder sample 1 by using the VSM-oven option of a Quantum Design PPMS setup of the Physical Measurements unit of the Servicio General de Apoyo a la Invesitigación-SAI, Universidad de Zaragoza. The powder was pressed into 3 mm diameter pellets of 3.1 and 2.8 mg for the two sets of measurements, which were performed to verify the reproducibility. The dc magnetization was determined in an applied field of 5 T, and the scan rate was 10 K min^{-1}, which was the smallest allowed by the setup. Several warming/cooling scans were performed, which showed only little variation between the first and second scan. The data reported here corresponds to the third stable and reproducible cycle of measurement. Corrections for the diamagnetism of the sample were calculated by using Pascal's constant.[36]

Differential scanning calorimetry

DSC measurements were performed with a Q1000 calorimeter from TA Instruments equipped with the LNCS accessory. The temperature and enthalpy scales were calibrated with a standard sample of indium, by using its melting transition (156.6 °C, 3296 J mol^{-1}). The measurements were carried out by using aluminum pans with a mechanical crimp, with an empty pan as reference. The zero-heat-flow procedure described by TA Instruments

was followed to derive heat capacities by using a synthetic sapphire as a reference compound. An overall accuracy of about 0.2 K for the temperature and up to 5 to 10 % for the heat capacity was estimated over the whole temperature range, by comparison with the synthetic sapphire. A lattice heat capacity was estimated from data below and above the anomaly that was associated with the SCO process (dashed line in Figure 4 b). Excess enthalpy and entropy were derived by integration of the excess heat capacity with respect to T and $\ln T$, respectively.

Modelling magnetic and calorimetric data with the domain model and the Slichter–Drickamer model

The phenomenological domain model, developed by Sorai,[26,27] was applied as it is widely used to analyze the SCO behavior in cases where calorimetric data are available. It is based on heterophase fluctuations and gives a measure of cooperativity through the number of like-spin molecules (or here the SCO centers) n per interacting domain; the larger the domain the more cooperative the transition. According to this model, the heat capacity variation can be written as in Equation (1):

$$\Delta C_p = \frac{n(\Delta_{\mathrm{SCO}}H)^2}{RT^2} \frac{\exp\left[\frac{n\Delta_{\mathrm{SCO}}H}{R}\left(\frac{1}{T}-\frac{1}{T_{1/2}}\right)\right]}{\left\{1+\exp\left[\frac{n\Delta_{\mathrm{SCO}}H}{R}\left(\frac{1}{T}-\frac{1}{T_{1/2}}\right)\right]\right\}^2} \tag{1}$$

The experimental heat capacity data were thus fitted to Equation (1) by using $\Delta_{\mathrm{SCO}}H$, as derived from integration of ΔC_p versus T, which gave $n=10.2/6.5$ and $T_{1/2}=434/415$ K upon warming and cooling, respectively. For $n=1$ the model is equivalent to a pure solution behavior (van't Hoff equation) with no cooperative effects.

A simple phenomenological expression [Eq. (2)], which is derived from the free energy of a regular solid solution of HS and LS molecules with an interaction term that is in accordance with mean-field theory, first used by Slichter and Drickamer,[16] reproduces well the different forms of SCO curves (γ_{HS} vs. T, in which γ_{HS} is the fraction of HS species) and also the hysteresis effect for sufficiently large values of the interaction parameter Γ. With the goal of attaining a mean-field estimation of cooperativity in the material under study, the experimental HS fraction calculated from magnetic measurements were fitted to Equation (2), and the thermodynamic figures were fixed to the ones determined by DSC.

$$\ln\left(\frac{1-\gamma_{HS}}{\gamma_{HS}}\right) = \frac{\Delta_{\mathrm{SCO}}H + \Gamma(1-2\gamma_{HS})}{RT} - \frac{\Delta_{\mathrm{SCO}}S}{R} \tag{2}$$

Because Equation (2) can only account for the amplitude of a hysteresis loop and not for its shape, it was considered that the vertical tangents of the calculated S-curve must correspond to $T_{1/2}\uparrow$ and $T_{1/2}\downarrow$.

The HS fraction γ_{HS} was deduced from the magnetic data by using the relation $\gamma_{\mathrm{HS}}(T) = (\chi_M T - \chi_M T_{\mathrm{LS}})/(\chi_M T_{\mathrm{HS}} - \chi_M T_{\mathrm{LS}})$, where $\chi_M T_{\mathrm{LS}}$ and $\chi_M T_{\mathrm{HS}}$ are the values of $\chi_M T$ in the LS and HS states, respectively. Values of 0.01 and 3.25 cm^3 mol^{-1} K were considered, respectively.

The HS fraction γ_{HS} was deduced from the calorimetric data by using the relation $\gamma_{\mathrm{HS}}(T) = \Delta H/\Delta_{\mathrm{SCO}}H$, in which $\Delta_{\mathrm{SCO}}H$ is the value derived by integration of the excess heat capacity versus T and multiplied by 1.05 to take into account the likely underestimation that is associated with few data above the heat capacity anomaly.

Computational Details

Vacuum and periodic density functional theory geometry optimizations and frequency calculations for both complexes have been performed by using the PBE functional[37] and POB-DZP basis set.[37] Vacuum calculations have been performed with the Turbomole 6.4 package,[38,39] whereas periodic calculations have been done by using Crystal14 (a shrinking factor of 4 was used for the k-point mesh; the LS state space group was $P\bar{1}$ and the HS state space group $C2/c$).[40] Single-point CASPT2 calculations were performed for the vacuum DFT-optimized structures of the complexes. For the CASPT2 calculations, the active space consisted of 10 electrons distributed over 12 orbitals, which included the five metal-centered 3d and 3d' orbitals and two ligand σ-orbitals.[41,42] The CASPT2 calculations were performed by using MOLCAS 7.4.[43,44] Scalar relativistic effects were included by using a Douglas–Kroll–Hess Hamiltonian and the basis set used in the calculations was the ANO-RCC basis set, which is designed to include relativistic effects.[45,46] The contracted Gaussian basis functions are (7s, 6p, 5d, 4f, 3g, 2h) for Fe, (4s, 3p, 1d) for N atoms bonded to Fe, (3s, 2p) for the remaining N atoms and C atoms, and (4s, 3p) for S and (2s) for H.

[1] P. Gütlich, H. A. Goodwin, *Top. Curr. Chem.* **2004**, *233*, 1–47.
[2] M. A. Halcrow, *Chem. Soc. Rev.* **2011**, *40*, 4119–4142.
[3] H. Spiering, T. Kohlhaas, N. Romstedt, A. Hauser, C. Bruns-Yilmaz, J. Kusz, P. Gütlich, *Coord. Chem. Rev.* **1999**, *190–192*, 629–647.
[4] O. Kahn, C. J. Martinez, *Science* **1998**, *279*, 44–48.
[5] B. Schäfer, C. Rajnak, I. Salitros, O. Fuhr, D. Klar, C. Schmitz-Antoniak, E. Weschke, H. Wende, M. Ruben, *Chem. Commun.* **2013**, *49*, 10986–10988.
[6] O. Roubeau, *Chem. Eur. J.* **2012**, *18*, 15230–15244.
[7] M. C. Muñoz, J. A. Real, *Coord. Chem. Rev.* **2011**, *255*, 2068–2093.
[8] Y. Raza, F. Volatron, S. Moldovan, O. Ersen, V. Huc, C. Martini, F. Brisset, A. Gloter, O. Stephan, A. Bousseksou, L. Catala, T. Mallah, *Chem. Commun.* **2011**, *47*, 11501–11503.
[9] R. Boča, M. Boca, L. Dlhan, K. Falk, H. Fuess, W. Haase, R. Jaroščiak, B. Papankova, F. Renz, M. Vrbova, *Inorg. Chem.* **2001**, *40*, 3025–3033.
[10] I. Šalitroš, N. T. Madhu, R. Boča, J. Pavlik, M. Ruben, *Monatsh. Chem.* **2009**, *140*, 695–733.
[11] L. Zhang, G.-C. Xu, H.-B. Xu, T. Zhang, Z.-M. Wang, M. Yuan, S. Gao, *Chem. Commun.* **2010**, *46*, 2554–2556.
[12] B. Weber, W. Bauer, J. Obel, *Angew. Chem. Int. Ed.* **2008**, *47*, 10098–10101; *Angew. Chem.* **2008**, *120*, 10252–10255.
[13] P. Guionneau, M. Marchivie, G. Bravic, J.-F. Létard, D. Chasseau, *Top. Curr. Chem.* **2004**, *234*, 97–128.
[14] B. Weber, W. Bauer, T. Pfaffeneder, M. M. Dîrtu, A. D. Naik, A. Rotaru, Y. Garcia, *Eur. J. Inorg. Chem.* **2011**, 3193–3206.
[15] M. A. Halcrow, *Chem. Lett.* **2014**, *43*, 1178–1188.
[16] C. P. Slichter, H. G. Drickamer, *J. Chem. Phys.* **1972**, *56*, 2142–2160.
[17] S. Bonnet, M. A. Siegler, J. S. Costa, G. Molnar, A. Bousseksou, A. L. Spek, P. Gamez, J. Reedijk, *Chem. Commun.* **2008**, 5619–5621.
[18] Z. Arcis-Castíllo, S. Zheng, M. A. Siegler, O. Roubeau, S. Bedoui, S. Bonnet, *Chem. Eur. J.* **2011**, *17*, 14826–14836.
[19] T. Norrby, A. Börje, L. Zhang, B. Åkermark, *Acta Chem. Scand.* **1998**, *52*, 77–85.
[20] J. Yin, B. Xiang, M. A. Huffman, C. E. Raab, I. W. Davies, *J. Org. Chem.* **2007**, *72*, 4554–4557.

[21] X. Bao, P.-H. Guo, W. Liu, J. Tucek, W.-X. Zhang, J.-D. Leng, X.-M. Chen, I. y. Gural'skiy, L. Salmon, A. Bousseksou, M.-L. Tong, *Chem. Sci.* **2012**, *3*, 1629 – 1633.

[22] M. B. Bushuev, V. A. Daletsky, D. P. Pishchur, Y. V. Gatilov, I. V. Korolkov, E. B. Nikolaenkova, V. P. Krivopalov, *Dalton Trans.* **2014**, *43*, 3906 – 3910.

[23] G. Schwarz, Y. Bodenthin, Z. Tomkowicz, W. Haase, T. Geue, J. Kohlbrecher, U. Pietsch, D. G. Kurth, *J. Am. Chem. Soc.* **2011**, *133*, 547 – 558.

[24] G. S. Matouzenko, S. A. Borshch, E. Jeanneau, M. B. Bushuev, *Chem. Eur. J.* **2009**, *15*, 1252 – 1260.

[25] R. Boča, F. Renz, M. Boča, H. Fuess, W. Haase, G. Kickelbick, W. Linert, M. Vrbová-Schikora, *Inorg. Chem. Commun.* **2005**, *8*, 227 – 230.

[26] M. Sorai, S. Seki, *J. Phys. Chem. Solids* **1974**, *35*, 555 – 570.

[27] M. Sorai, *Top. Curr. Chem.* **2004**, *235*, 153 – 170.

[28] M. Sorai, Y. Nakazawa, M. Nakano, Y. Miyazaki, *Chem. Rev.* **2012**, *113*, PR41 – PR122.

[29] A. Hauser, C. Enachescu, M. L. Daku, A. Vargas, N. Amstutz, *Coord. Chem. Rev.* **2006**, *250*, 1642 – 1652.

[30] A. Vef, U. Manthe, P. Gutlich, A. Hauser, *J. Chem. Phys.* **1994**, *101*, 9326 – 9332.

[31] A. Rudavskyi, C. Sousa, C. de Graaf, R. W. A. Havenith, R. Broer, *J. Chem. Phys.* **2014**, *140*, 184318.

[32] M. Gruden-Pavlović, S. Stepanović, M. Perić, M. Güell, M. Swart, *Phys. Chem. Chem. Phys.* **2014**, *16*, 14514 – 14522.

[33] O. Salomon, M. Reiher, B. A. Hess, *J. Chem. Phys.* **2002**, *117*, 4729 – 4737.

[34] M. Reiher, O. Salomon, B. A. Hess, *Theor. Chem. Acc.* **2001**, *107*, 48 – 55.

[35] G. M. Sheldrick, *Acta Crystallogr. C* **2015**, *71*, 3 – 8.

[36] G. A. Bain, J. F. Berry, *J. Chem. Educ.* **2008**, *85*, 532 – 536.

[37] J. P. Perdew, K. Burke, M. Ernzerhof, *Phys. Rev. Lett.* **1996**, *77*, 3865 – 3868.

[38] O. Treutler, R. Ahlrichs, *J. Chem. Phys.* **1995**, *102*, 346 – 354.

[39] M. von Arnim, R. Ahlrichs, *J. Comput. Chem.* **1998**, *19*, 1746 – 1757.

[40] R. Dovesi, V. R. Saunders, C. Roetti, R. Orlando, C. M. Zicovich-Wilson, F. Pascale, B. Civalleri, K. Doll, N. M. Harrison, I. J. Bush, P. D'Arco, M. Llunell, M. Causà, Y. Noël, *CRYSTAL14 User's Manual*, University of Torino, Torino, **2014**.

[41] K. Andersson, B. O. Roos, *Chem. Phys. Lett.* **1992**, *191*, 507 – 514.

[42] C. D. Graaf, R. Broer, W. C. Nieuwpoort, *Chem. Phys.* **1996**, *208*, 35 – 43.

[43] G. Karlström, R. Lindh, P. A. Malmqvist, B. O. Roos, U. Ryde, V. Veryazov, P. O. Widmark, M. Cossi, B. Schimmelpfennig, P. Neogrady, L. Seijo, *Comput. Mater. Sci.* **2003**, *28*, 222 – 239.

[44] F. Aquilante, L. D. Vico, N. Ferré, G. Ghigo, P. Å. Malmqvist, P. Neogrády, T. B. Pedersen, M. Pitonak, M. Reiher, B. O. Roos, L. Serrano-Andrés, M. Urban, V. Veryazov, R. Lindh, *J. Comput. Chem.* **2010**, *31*, 224 – 247.

[45] M. Douglas, N. M. Kroll, *Ann. Phys* **1974**, *82*, 89 – 155.

[46] B. A. Hess, *Phys. Rev. A* **1986**, *33*, 3742 – 3748.

[47] A. L. Spek, *Acta Crystallogr.* **2009**, *D65*, 148 – 155.

[48] H. D. Flack, *Acta Crystallogr.* **1983**, *A39*, 876 – 881.